


Cite this: *RSC Adv.*, 2017, 7, 25650

# Loading of $\text{Co}_3\text{O}_4$ onto Pt-modified nitrogen-doped $\text{TiO}_2$ nanocomposites promotes photocatalytic hydrogen production†

Wen-Dong Wei, Xiang-Yu Liu, Shi-Cong Cui\* and Jin-Gang Liu \*

Photocatalytic water splitting has been considered as one of the most promising methods to produce hydrogen as a source of clean fuel. Use of co-catalysts and elemental doping in  $\text{TiO}_2$  has been extensively explored for effective photocatalysis. Here we report the synthesis of visible light responsive Pt and  $\text{Co}_3\text{O}_4$  co-modified nitrogen-doped  $\text{TiO}_2$  (N- $\text{TiO}_2$ ) nanocomposites for efficient photocatalytic hydrogen production. Pt- $\text{Co}_3\text{O}_4$ (S)/N- $\text{TiO}_2$  (PCNT(S)) and Pt- $\text{Co}_3\text{O}_4$ (D)/N- $\text{TiO}_2$  (PCNT(D)) composites were synthesized by one- and two-step methods, respectively. Experimental results showed that additional loading of  $\text{Co}_3\text{O}_4$  onto a very low content (0.02 wt%) Pt-modified N- $\text{TiO}_2$  nanocomposite significantly increases the efficiency of photocatalytic hydrogen production. Catalyst composites prepared by the two-step method, where close interaction occurred between the surface-loaded  $\text{Co}_3\text{O}_4$  and Pt on the N- $\text{TiO}_2$  nanoparticles, showed much higher photocatalytic activity for hydrogen production than that prepared by the one-step method, where  $\text{Co}_3\text{O}_4$  is evenly dispersed in N- $\text{TiO}_2$ . The position of the co-catalyst  $\text{Co}_3\text{O}_4$  in  $\text{TiO}_2$  has a significant effect on the photocatalytic properties of the prepared photocatalysts.

Received 19th March 2017

Accepted 5th May 2017

DOI: 10.1039/c7ra03216a

rsc.li/rsc-advances

## 1 Introduction

Nowadays, cleaner renewable energy production has become the most prevailing global issue owing to the growing demand for nonrenewable fossil fuels and the environmental pollution caused by these fossil fuels.<sup>1</sup> Recently, hydrogen ( $\text{H}_2$ ), as a secondary source of energy, has been proved to be a promising fuel and energy carrier owing to its renewability, no pollution, ideal calorific value, and universal element properties.<sup>2–5</sup> Photocatalytic water splitting has been considered as one of the most promising methods to produce  $\text{H}_2$  because of its environmentally benign process and the use of solar energy as an energy source.<sup>6–8</sup> The process was originally discovered by Fujishima and Honda in 1972 through photoelectrochemical water splitting by  $\text{TiO}_2$  single crystal electrodes under ultraviolet (UV) light radiation.<sup>9</sup> Since then,  $\text{TiO}_2$  has drawn immense attraction of researchers to water splitting by photoelectrochemical or photocatalytic systems.<sup>10</sup>

Nevertheless, the large bandgap (3.2 eV) and high photo-generated electron-hole recombination rate constrain the practical use of  $\text{TiO}_2$  in the  $\text{H}_2$  evolution reaction.<sup>11,12</sup> Elemental

doping is an effective way to decrease the semiconductor bandgap.<sup>13–15</sup> Nitrogen-doped (N-doped)  $\text{TiO}_2$  has widely been used in photocatalytic water splitting, which showed efficient  $\text{H}_2$  production under visible light irradiation by narrowing the bandgap energy of  $\text{TiO}_2$ .<sup>16,17</sup> At the same time, application of co-catalyst was found to be effective in reducing the recombination of photo generated electron and holes.<sup>18,19</sup> Thus far, many studies have reported that loading of noble metals such as Au,<sup>20,21</sup> Ag,<sup>22</sup> Pt,<sup>23</sup> and Rh<sup>24</sup> on the surface of a semiconductor as a co-catalyst plays an important role in photocatalytic water splitting, which revealed that high  $\text{H}_2$  production is due to the electron trapping properties of noble metals. Application of Pt has been extensively studied because an appropriate Schottky barrier is found in it, which is beneficial for  $\text{H}^+$  reduction.<sup>25–27</sup> Yu *et al.*<sup>28</sup> fabricated Pt/ $\text{TiO}_2$  by the photochemical reduction of  $\text{H}_2\text{PtCl}_6$  on  $\text{TiO}_2$  and found that the rate of photocatalytic  $\text{H}_2$  production was significantly enhanced by loading Pt on the surface of  $\text{TiO}_2$ , and the optimal content of Pt loading was about 2.0 wt%. In addition to noble metals, cobalt oxide has recently been explored as an alternative co-catalyst for photocatalytic  $\text{H}_2$  production.<sup>29,30</sup> Bala *et al.*<sup>31</sup> synthesized the  $\text{Co}_3\text{O}_4/\text{TiO}_2$  composite using Co(II) metal-organic frameworks as a  $\text{TiO}_2$  absorbent and sacrificial template, in which  $\text{Co}_3\text{O}_4$  acted as a co-catalyst to extract the photogenerated charge carrier, exhibiting high  $\text{H}_2$  evolution rate. However, to the best of our knowledge, no example has been reported about the synergistic effect of different co-catalysts on the  $\text{H}_2$  evolution rate of related  $\text{TiO}_2$ -based photocatalysts.

Key Laboratory for Advanced Materials, School of Chemistry & Molecular Engineering, East China University of Science and Technology, Shanghai 200237, P. R. China.  
E-mail: shicongcui@ecust.edu.cn; liujingang@ecust.edu.cn

† Electronic supplementary information (ESI) available: TEM images of other samples, data of photocatalytic water splitting, and BET of surface areas of all samples. See DOI: 10.1039/c7ra03216a



In this study, we have used two different methods to prepare Pt and  $\text{Co}_3\text{O}_4$  co-modified N-doped  $\text{TiO}_2$  ( $\text{N-TiO}_2$ ) composites and investigated the  $\text{H}_2$  evolution from water photocatalyzed by these composites. Results showed that the presence of  $\text{Co}_3\text{O}_4$  on very low content Pt-modified  $\text{N-TiO}_2$  composite further enhanced the photocatalytic efficiency as compared to the Pt-only-modified composite,  $\text{Pt@N-TiO}_2$ . Moreover, the position of the  $\text{Co}_3\text{O}_4$  particles on the composite has a significant effect on the photocatalytic activity of the catalyst.

## 2 Experimental methods

### 2.1 Preparation of $\text{N-TiO}_2$

All chemicals used in this study were of analytical grade and used as received without further purification. In the typical synthetic procedure, tetrabutyltitanate (TBOT, 0.029 mol) was added to 30 mL of isopropanol with magnetic stirring. Then, 40 mL of acetic acid solution ( $V_{\text{CH}_3\text{COOH}} : V_{\text{H}_2\text{O}} = 1 : 3$ ) was added dropwise to the above mixture and kept in an ice bath until a white precipitate was obtained. After stirring the solution continuously for 3 h to complete the hydrolysis, a certain amount of choline was added till the pH of the solution reached 9.0. The precursor was then transferred into a 50 mL Teflon-lined autoclave and heated at 180 °C for 24 h in an oven. Then, it was allowed to cool to room temperature naturally. A yellowish-white precipitate was obtained after centrifuging the solution, and the precipitate was washed several times with water and ethanol and dried at 60 °C overnight. The obtained composite was further annealed at 300 °C for 3 h (2 °C  $\text{min}^{-1}$ ) under air atmosphere to afford  $\text{N-TiO}_2$ .

### 2.2 Preparation of $\text{Co}_3\text{O}_4/\text{N-TiO}_2$

The  $\text{Co}_3\text{O}_4/\text{N-TiO}_2$  composites were synthesized by two different methods: two-step and one-step methods. The composites prepared by the two-step method were represented as  $\text{Co}_3\text{O}_4(\text{D})/\text{N-TiO}_2$  (CNT(D)). The  $\text{Co}_3\text{O}_4$  co-catalyst was loaded onto  $\text{N-TiO}_2$  through impregnation of aqueous  $\text{Co}(\text{NO}_3)_2$  solution on the  $\text{N-TiO}_2$  nanoparticles. About 0.5 mL of aqueous  $\text{Co}(\text{NO}_3)_2$  solution with different concentrations (25, 62.5, 125, and 312.5  $\text{mmol L}^{-1}$ ) was slowly added to 0.5 g of  $\text{N-TiO}_2$  powder, and the resultant composite was left for several hours till the powder was thoroughly soaked. The impregnated powder was dried at 60 °C and calcined under air atmosphere at 300 °C for 3 h (2 °C  $\text{min}^{-1}$ ). In  $\text{Co}_3\text{O}_4/\text{N-TiO}_2$  composites having different concentrations of  $\text{Co}(\text{NO}_3)_2$ , the molar ratios of Co : Ti atoms were 0.002, 0.005, 0.01, and 0.025, respectively, and they were represented as CNT(D)-1, CNT(D)-2, CNT(D)-3, and CNT(D)-4, respectively.

The  $\text{Co}_3\text{O}_4/\text{N-TiO}_2$  composites synthesized by the one-step method were represented as  $\text{Co}_3\text{O}_4(\text{S})/\text{N-TiO}_2$  (CNT(S)). First, TBOT (0.029 mol) and different amounts of cobalt nitrate hexahydrate ( $\text{Co}(\text{NO}_3)_2 \cdot 6\text{H}_2\text{O}$ ) were added to 30 mL of isopropanol with constant magnetic stirring. The procedure was the same as that described for the two-step method in Section 2.1. However, the molar ratios of Co : Ti atoms (Co : Ti = 0.002, 0.005, 0.01, and 0.025) were adjusted by controlling the

concentration of  $\text{Co}(\text{NO}_3)_2$  solution (25 mM to 0.31 M) during the preparation process. The composites thus prepared were labeled as CNT(S)-1, CNT(S)-2, CNT(S)-3, and CNT(S)-4, respectively.

### 2.3 Preparation of $\text{Pt-Co}_3\text{O}_4/\text{N-TiO}_2$

The  $\text{Pt-Co}_3\text{O}_4/\text{N-TiO}_2$  composites were prepared by *in situ* photoreduction of  $\text{H}_2\text{PtCl}_6$  on  $\text{Co}_3\text{O}_4/\text{N-TiO}_2$  under light irradiation. CNT(S) or CNT(D) powder (1.0 g) was dispersed in a  $\text{H}_2\text{PtCl}_6$  solution (100 mL, 0.01  $\text{mmol L}^{-1}$ ) to produce the Pt 0.02 wt% loaded  $\text{Co}_3\text{O}_4(\text{S})/\text{N-TiO}_2$  (PCNT(S)) or the Pt 0.02 wt% loaded  $\text{Co}_3\text{O}_4(\text{D})/\text{N-TiO}_2$  (PCNT(D)). The different loading amount of Pt in the system was controlled by changing the concentration of the  $\text{H}_2\text{PtCl}_6$  solution. The resulting suspension was stirred and irradiated by a 300 W Xe arc lamp for 1 h in a top-irradiation cell with a Pyrex window. The composites were then centrifuged and freeze dried.

### 2.4 Characterizations

The morphology and structure of these composites were analyzed through transmission electron microscopy (TEM) and high-resolution transmission electron microscopy (HRTEM) with a JEOL model JEM 2100 EX instrument at an acceleration voltage of 200 kV. X-ray powder diffraction (XRD) was performed with a Rigaku Dmax-3C diffractometer using Cu K $\alpha$  radiation ( $\lambda = 0.15408 \text{ nm}$ ) operated at 40 kV and 20 mA to characterize the crystal phases and crystallinity of the samples. Ultraviolet-visible (UV-Vis) absorption spectra of the samples were recorded by a Shimadzu UV-2600 spectrophotometer at a wavelength of 1000–200 nm. The photoluminescence (PL) spectra were measured using a fluorospectrophotometer (Horiba Fluoromax-4) at room temperature. The chemical states of surface elements were analyzed by X-ray photoelectron spectroscopy (XPS; Perkin-Elmer PHI 5000C).

### 2.5 Photocatalytic hydrogen production

During water splitting for the evolution of  $\text{H}_2$ , photocatalytic activity was evaluated under visible light and full spectrum irradiation. Photocatalytic experiments were performed in a gas-closed system using a Pyrex cell with a top quartz window. Typically, 100 mg of photocatalyst powder was ultrasonically dispersed in 100 mL of aqueous solution containing methanol as a sacrificial agent ( $V_{\text{H}_2\text{O}} : V_{\text{MeOH}} = 9 : 1$ ). Before irradiation, the system was evacuated several times to remove the residual air completely and then irradiated from the top window using a 300 W Xe lamp and a UV light cutoff filter ( $\lambda > 400 \text{ nm}$ ) with a light intensity of 380  $\text{mW cm}^{-2}$ . The reaction temperature was maintained at 25 °C with a water cooling circulator. The reaction was performed for 6 h, and the  $\text{H}_2$  gas produced was analyzed by a gas chromatograph (SHIMADZU GC-2014) equipped with a thermal conductivity detector. The sample of the gaseous mixture (2.0 mL) was drawn from the online sampling loop and argon was used as the carrier gas. Control experiments were performed without and with photocatalysts under light irradiation and in the dark, respectively.



## 3 Results and discussions

### 3.1 Morphologies and structures

The micromorphology and structures of the catalysts PCNT(D)-2 and PCNT(S)-2 with best photocatalytic performance were analyzed by TEM and HRTEM. In Fig. 1a, PCNT(D)-2 was shown with TiO<sub>2</sub> nanoparticles that have an average diameter of 17 nm. There were also other small particles attached to the TiO<sub>2</sub> nanoparticles, indicating the presence of Co<sub>3</sub>O<sub>4</sub> on the surface of TiO<sub>2</sub>. Fig. 1b displayed the HRTEM image of PCNT(D)-2. A lattice spacing of 0.35 nm matched well with the (101) crystal plane of anatase TiO<sub>2</sub>. Moreover, a lattice fringe of 0.24 nm indicated that the bare crystal of (311) plane over Co<sub>3</sub>O<sub>4</sub> emerged,<sup>32</sup> revealing the successful loading of Co<sub>3</sub>O<sub>4</sub>. When Pt-Co<sub>3</sub>O<sub>4</sub>/N-TiO<sub>2</sub> was prepared by the one-step method, an average particle diameter of 12 nm ranging from 9 to 16 nm were obtained, which may be due to the disturbance of Co during the formation of TiO<sub>2</sub>. A lattice spacing of 0.37 nm corresponded to anatase TiO<sub>2</sub> (101) crystal plane (Fig. 1d).<sup>33,34</sup> No other crystal was found in the HRTEM image of PCNT(S)-2, indicating that Co<sub>3</sub>O<sub>4</sub> were probably dispersed in the N-TiO<sub>2</sub> particles rather than loaded onto the surface of N-TiO<sub>2</sub>. No Pt particle was found in either sample, suggesting the low content of Pt in the composites.

### 3.2 XRD analysis

With the help of XRD measurements, the crystal phases of the samples were evaluated. Fig. 2a displayed the XRD patterns of PCNT(D). In the case of N-TiO<sub>2</sub>, all the diffraction peaks around  $2\theta = 25.28^\circ, 37.80^\circ, 48.05^\circ, 53.89^\circ, 55.06^\circ, 62.69^\circ, 68.76^\circ, 70.31^\circ$ , and  $75.03^\circ$  were attributed to (101), (004), (200), (105), (211), (204), (116), (220), and (215) crystal planes of anatase TiO<sub>2</sub> (JCPDS card no. 21-1272),<sup>35,36</sup> respectively. Different from N-TiO<sub>2</sub>, a small portion of anatase TiO<sub>2</sub> began to transfer to brookite TiO<sub>2</sub> when 0.002 of Co was introduced. The diffraction peaks at  $30.81^\circ, 36.25^\circ$ , and  $40.15^\circ$ , which were in accordance with (121), (012),

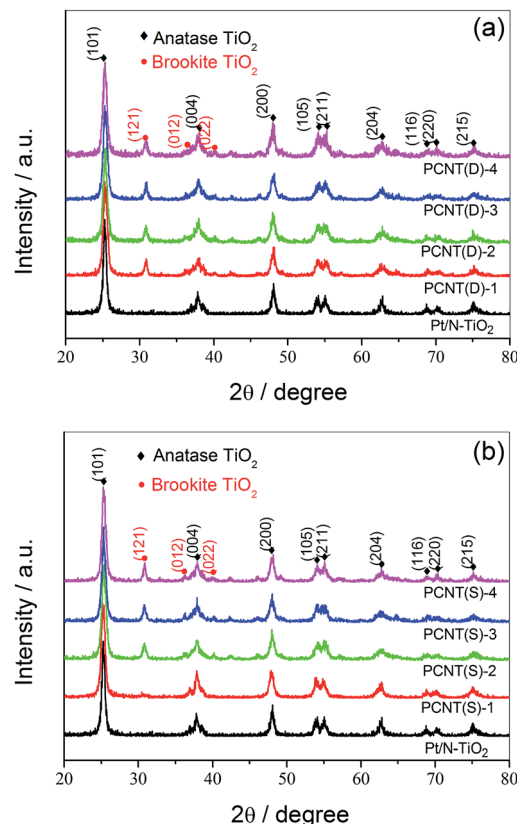


Fig. 2 X-ray powder diffraction patterns of PCNT(D) (a) and PCNT(S) (b).

and (022) lattice planes of brookite TiO<sub>2</sub>, respectively, confirmed the existence of brookite.<sup>37</sup> As shown in Fig. 2b, no brookite TiO<sub>2</sub> was observed till the amount of Co was about 0.005 in PCNT(S) (PCNT(S)-2), which was different from that of PCNT(D). By increasing the Co content from 0.002 to 0.005, brookite was found in TiO<sub>2</sub>, indicating the co-existence of both anatase and brookite TiO<sub>2</sub>. The presence of Co<sub>3</sub>O<sub>4</sub> probably affects the rearrangement of the atoms in TiO<sub>2</sub> thus promoting anatase to brookite transformation during the crystal formation process. This phenomenon has also been found in other publications.<sup>38,39</sup> It was reported that TiO<sub>2</sub> mixture containing both anatase and brookite revealed excellent thermal stability, which might be a valuable factor for the high efficiency of photocatalytic water splitting.<sup>40</sup> Moreover, no typical diffraction peaks assignable to Pt- and Co-based components were detected, which may be because of their low content.

### 3.3 UV-Vis diffuse reflectance spectroscopy analysis

The optical properties of the samples were investigated by UV-Vis diffuse reflectance spectroscopy (DRS), and the corresponding bandgap energies ( $E_g$ ) were estimated by the Kubelka-Munk plots.<sup>41</sup> Fig. 3a shows the DRS spectra of N-TiO<sub>2</sub>, Pt/N-TiO<sub>2</sub> and PCNT(D), from which we could observe that N-TiO<sub>2</sub> exhibited slight visible light absorption. After loading Co<sub>3</sub>O<sub>4</sub> to N-TiO<sub>2</sub>, the absorption of the PCNT(D) composites in visible region further increased. The composites showed prominent

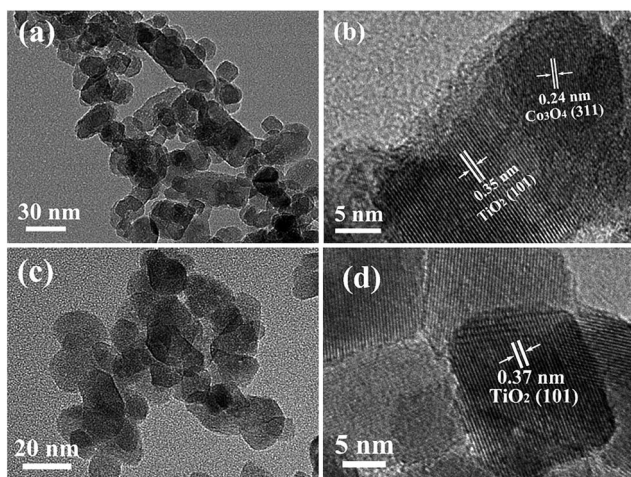


Fig. 1 Transmission electron microscope and high-resolution transmission electron microscopic images of PCNT(D)-2 (a and b) and PCNT(S)-2 (c and d).



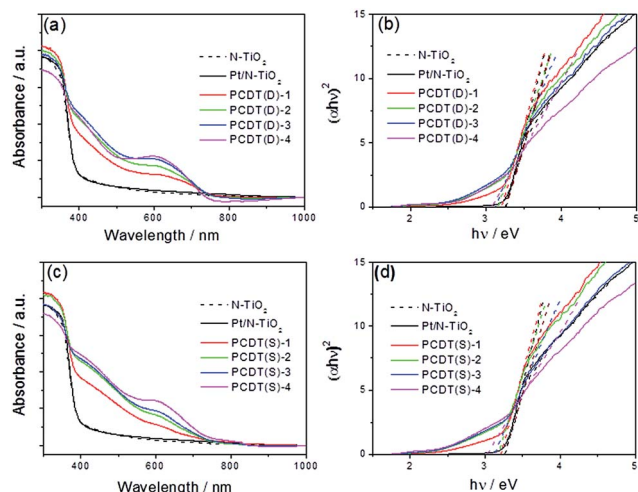


Fig. 3 Ultraviolet-visible (UV-Vis) diffuse reflectance spectra (a and c) and the corresponding Kubelka–Munk plots (b and d) of PCNT(D) (a and b) and PCNT(S) (c and d) with different amounts of Co<sub>3</sub>O<sub>4</sub>.

light absorption in the range of 400–700 nm, which was mainly attributed to the  $\text{O}^{2-} \rightarrow \text{Co}^{3+}$  and  $\text{O}^{2-} \rightarrow \text{Co}^{2+}$  transitions of loaded Co<sub>3</sub>O<sub>4</sub> that has small band gaps.<sup>42,43</sup> With the increase of Co content, the absorption intensity increased gradually, particularly in the region from 500 to 700 nm. The  $E_g$  values of TiO<sub>2</sub> in Pt/N-TiO<sub>2</sub>, PCNT(D)-1, PCNT(D)-2, PCNT(D)-3, and PCNT(D)-4 were estimated to be 3.26, 3.21, 3.16, 3.13, and 3.08 eV, respectively (Fig. 3b). The samples prepared by two-step method showed similar UV-Vis absorption as that prepared by the one-step method (Fig. 3c). As shown in Fig. 3d, the  $E_g$  values of TiO<sub>2</sub> in N-TiO<sub>2</sub>, PCNT(S)-1, PCNT(S)-2, PCNT(S)-3, and PCNT(S)-4 were 3.26, 3.21, 3.17, 3.12, and 3.02 eV, respectively. Obviously, loading Co<sub>3</sub>O<sub>4</sub> to the composite promotes the catalyst for higher visible light absorption. This would beneficially contribute to the photo-activity of the composite under visible light irradiation. While, it should be noted that the catalyst composite with the best catalytic activity is not the one with the most visible light absorption as observed in this study for the H<sub>2</sub> production. Similar phenomena have also been reported by other researchers.<sup>44,45</sup>

### 3.4 PL behavior

The photocatalytic activity of photocatalysts is usually closely associated with the separation and recombination behavior of the photogenerated electrons and holes.<sup>46,47</sup> PL spectra of PCNT(D) and PCNT(S) with different amounts of Co were then measured. From Fig. 4a and b, it was obvious that the PL intensities of PCNT(D) and PCNT(S) were significantly smaller than that of Pt/N-TiO<sub>2</sub>. For the PCNT catalyst composites, the photogenerated electrons in the conduction band of N-TiO<sub>2</sub> could transfer into the energy level of modified Co<sub>3</sub>O<sub>4</sub>, which may reduce the radiative recombination efficiency of photogenerated electrons and holes. This indicates that loading Co<sub>3</sub>O<sub>4</sub> on the catalyst composite separates the photogenerated charge carriers effectively, which is beneficial for the photocatalytic activity.

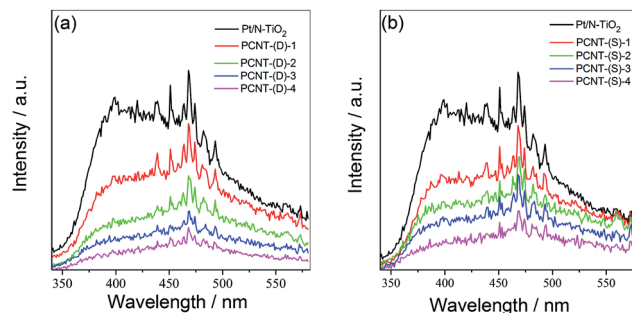


Fig. 4 Photoluminescence (PL) spectra of PCNT(D) (a) and PCNT(S) (b) with different Co contents.

### 3.5 XPS analysis

XPS spectra were measured to investigate the surface chemical components and chemical states of the samples. Fig. 5 showed the XPS spectra of Pt/N-TiO<sub>2</sub>, PCNT(D)-2, and PCNT(S)-2. In Fig. 5a, the XPS survey spectra showed that Pt/N-TiO<sub>2</sub> contained Ti, O, N, and Pt elements, whereas both PCNT(D)-2 and PCNT(S)-2 contained Ti, O, N, Pt, and Co elements due to the introduction of Co. High-resolution XPS spectra of Pt 4f and Co 2p were shown in Fig. 5b and c, respectively. The Pt 4f band of Pt/N-TiO<sub>2</sub> and PCNT(S)-2 was divided into two Gaussian–Lorentzian peaks with binding energies at around 74.9 and 76.8 eV, respectively, corresponding to metallic (Pt<sup>0</sup>) Pt 4f<sub>7/2</sub> and 4f<sub>5/2</sub> states.<sup>48</sup> The blue shifts of the Pt peaks in PCNT(D)-2 (74.4 and 75.7 eV) and PCNT(S)-2 (75.0 and 76.5 eV) were compared (Fig. 5b). This could be attributed to the interaction of Co in Co<sub>3</sub>O<sub>4</sub> with Pt on the surface of PCNT(D)-2. As shown in Fig. 5c, Co was detected in both PCNT(D)-2 and PCNT(S)-2. The peaks of Co in PCNT(D)-2 were found at approximate 780.8 and 795.7 eV which were assignable to the binding energies of Co 2p<sub>3/2</sub> and 2p<sub>1/2</sub>.<sup>49</sup> While the binding energies for Co in PCNT(D)-2 were found at about 783.3 and 796.6 eV, which shifted to higher energy relative to PCNT(S)-2, suggesting the interaction between Co<sub>3</sub>O<sub>4</sub> and Pt.<sup>50</sup>

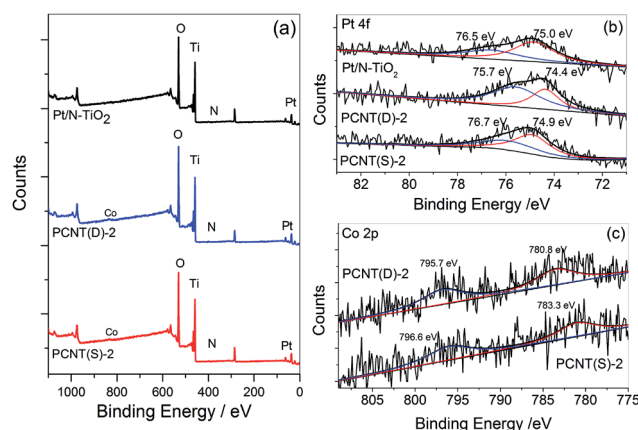


Fig. 5 X-ray photoelectron spectra (XPS) of Pt/N-TiO<sub>2</sub>, PCNT(D)-2, and PCNT(S)-2 for survey (a), Pt 4f (b), and Co 2p (c).



XPS etching was then employed to explore the existence of Co in PCNT(D)-2 and PCNT(S)-2. The Co contents on the surface and 5 nm inside PCNT(D)-2 were 2.39 and 2.01 at%, respectively. The larger content of Co on the surface than that in the interior could be ascribed to the additional loading of  $\text{Co}_3\text{O}_4$  on the surface of N-TiO<sub>2</sub>. On the other hand, in the case of PCNT(S)-2, both values were essentially the same, 1.02 and 1.03 at%, respectively. The XPS etching results indicated that  $\text{Co}_3\text{O}_4$  was evenly dispersed in N-TiO<sub>2</sub> when prepared by the one-step method, but it was mainly loaded on the surface of N-TiO<sub>2</sub> when synthesized by the two-step method.

### 3.6 Water splitting activity

The effects of Pt loading amount on the H<sub>2</sub> evolution rate of CNT(D)-2 and CNT(S)-2 under UV-Vis and visible light irradiation were shown in Fig. 6. The H<sub>2</sub> evolution rates of CNT(D)-2 and CNT(S)-2 under UV-Vis light varied with the Pt-loading amount. It was clearly shown that additional loading of  $\text{Co}_3\text{O}_4$  onto appropriate amount of Pt modified N-TiO<sub>2</sub> composite remarkably improved the photocatalytic efficiency for H<sub>2</sub> production (Fig. 6a, Table S1†), which signifies the important contribution from the loaded  $\text{Co}_3\text{O}_4$ . It is interesting to note that CNT(D)-2 exhibited higher H<sub>2</sub> evolution rates in all cases than CNT(S)-2. The maximum differences of H<sub>2</sub> production rates were obtained with a Pt loading of 0.02 wt% in both CNT(D)-2 and CNT(S)-2, which revealed the optimal concentration of Pt loading. With Pt loading higher than 0.02 wt%, the rate of H<sub>2</sub> evolution declined quickly at 0.2 wt%. The same trend was observed when the samples were irradiated under visible light (Fig. 6b, Table S2†). The higher catalytic activity of CNT(D)-2 than CNT(S)-2 could be attributed to the synergistic effect played by the closely contacted Pt with  $\text{Co}_3\text{O}_4$  on the surface of N-TiO<sub>2</sub>.

The effect of Co contents on the photocatalytic performance of PCNT(D) and PCNT(S) was then investigated. Fig. 7a showed the H<sub>2</sub> evolution rate of PCNT(D) and PCNT(S) with different Co contents under visible light irradiation ( $\lambda > 400$  nm). It was clear that the H<sub>2</sub> evolution rate of PCNT(D) increased with the increase in Co contents from 0.002 to 0.005 and then decreased with further increase in Co content to 0.025. The H<sub>2</sub> evolution rate achieved a maximum value of  $197 \mu\text{mol g}^{-1} \text{h}^{-1}$  at 0.005 content, suggesting optimal Co content. In addition, it was noteworthy that when Co content increased to 0.025, the H<sub>2</sub> evolution rate rapidly decreased to  $32 \mu\text{mol g}^{-1} \text{h}^{-1}$ . The extremely low

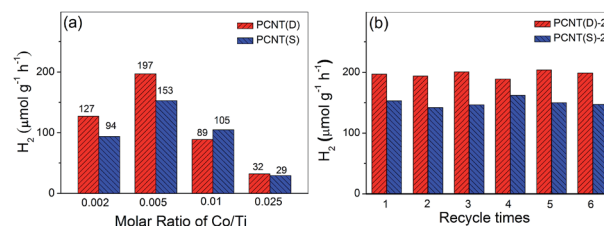


Fig. 7 Photocatalytic H<sub>2</sub> evolution of PCNT(D) and PCNT(S) versus different amounts of Co (a), and photocatalytic H<sub>2</sub> evolution in six-run recycling experiments using PCNT(D)-2, and PCNT(S)-2 composites (b).

H<sub>2</sub> production was probably due to the formation of vast crystal defects, which greatly promoted the recombination of photoelectrons and holes. A similar trend was observed in PCNT(S) samples with different Co contents, in which Co content at 0.005 showed the highest H<sub>2</sub> evolution (Fig. 7a, Table S3†). The stability of the photocatalysts was investigated by a six-run recycling experiment of H<sub>2</sub> evolution under similar conditions. PCNT(D) showed higher photocatalytic activities as compared to PCNT(S). As shown in Fig. 7b, after six-run cycles, H<sub>2</sub> evolution, catalyzed by PCNT(D) and PCNT(S), mainly remained as high as the initial, suggesting the excellent stabilities of both PCNT(D) and PCNT(S).

Taken all the experimental results together, it can be concluded that loading of  $\text{Co}_3\text{O}_4$  on Pt/N-TiO<sub>2</sub> composite significantly promotes the PCNT catalysts photocatalytic activity, and PCNT(D) showed much higher H<sub>2</sub> evolution rates than PCNT(S) composites under the same Pt-loading content. This indicates that the existing state of  $\text{Co}_3\text{O}_4$  in the composites played a crucial role in the photocatalytic performance of the catalyst. XPS spectra and TEM images of the composites showed the distribution of  $\text{Co}_3\text{O}_4$  in PCNT(D) and PCNT(S), where  $\text{Co}_3\text{O}_4$  was located on the surface of N-TiO<sub>2</sub> in PCNT(D) (Fig. 8a) and was evenly dispersed in N-TiO<sub>2</sub> in the case of PCNT(S) (Fig. 8b). For the PCNT(D) composites (Fig. 8a), visible light irradiation of N-TiO<sub>2</sub> produces photogenerated electrons and holes; the generated electrons are then captured by the closely contacted Pt/ $\text{Co}_3\text{O}_4$  particles on which water splits to produce hydrogen, and the holes were consumed by reacting with the sacrificial donor reagent. In the case of PCNT(S) composites,  $\text{Co}_3\text{O}_4$  and Pt were

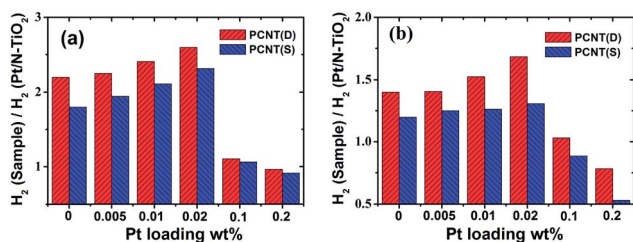


Fig. 6 Effects of different amounts of Pt loading on H<sub>2</sub> evolution rate of PCNT(D) and PCNT(S) under UV-Vis (a) and visible light (b) irradiation, respectively.

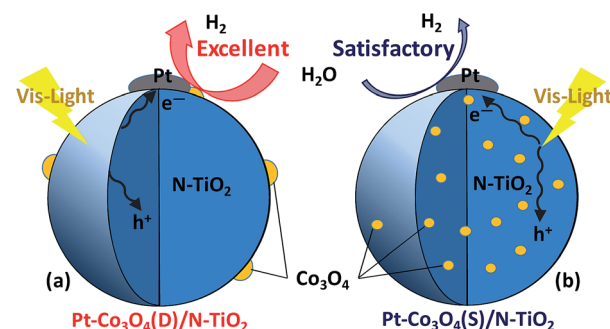


Fig. 8 Pictorial depiction of the existence of  $\text{Co}_3\text{O}_4$  in PCNT(D) (a) and PCNT(S) (b).



located separately on the surface of N-TiO<sub>2</sub> lacking of direct interaction (Fig. 8b), in which charge separation efficiency would be lower than that in the PCNT(D) composites when photo-irradiated. Accordingly, when appropriate amounts of Co<sub>3</sub>O<sub>4</sub> and Pt were loaded onto the surface of N-TiO<sub>2</sub> nanoparticles, the close interaction between Co<sub>3</sub>O<sub>4</sub> and Pt may provide more effective electric transmission, showing synergistic effect for promoting the separation of photogenerated electrons and holes and thus boosting the photocatalytic activity.

## 4 Conclusions

The visible light responsive photocatalysts PCNT(S) and PCNT(D) were synthesized successfully by one-step and two-step methods, respectively. Compared with the Pt@N-TiO<sub>2</sub> catalyst, Co<sub>3</sub>O<sub>4</sub>-modified composites show significant improvements in the photocatalytic performance for H<sub>2</sub> production with very low loading of Pt (0.02 wt%). Catalyst composites prepared by the two-step method showed higher photocatalytic activity for H<sub>2</sub> production than that prepared by the one-step method. The two-step method led to close interaction between the loaded Co<sub>3</sub>O<sub>4</sub> and Pt on the N-TiO<sub>2</sub> nanoparticles, whereas the one-step method produced composites with Co<sub>3</sub>O<sub>4</sub> evenly dispersed in N-TiO<sub>2</sub>. The methods of preparation and thus the co-catalyst distribution in TiO<sub>2</sub> have a strong influence on the catalytic properties of the prepared composites. The results obtained may have implications for further development of high-performance catalysts for photocatalytic H<sub>2</sub> production.

## Acknowledgements

This study was financially supported by the NSF of China (no. 21271072, 21571062 to JGL; 21571063 to SCC), the Program for Professor of Special Appointment (Eastern Scholar) at Shanghai Institutions of Higher Learning to JGL, and the Fundamental Research Funds for the Central Universities (no. 222201717003).

## Notes and references

- 1 M. Y. Liu, W. Zhou, T. Wang, D. F. Wang, L. Q. Liu and J. H. Ye, *Chem. Commun.*, 2016, **52**, 4694–4697.
- 2 D. F. Su, J. Wang, H. Y. Jin, Y. T. Gong, M. M. Li, Z. F. Pang and Y. Wang, *J. Mater. Chem. A*, 2015, **3**, 11756–11761.
- 3 M. Z. Ge, C. Y. Cao, S. H. Li, Y. X. Tang, L. N. Wang, N. Qi, J. Y. Huang, K. Q. Zhang, S. S. Al-Deyabe and Y. K. Lai, *Nanoscale*, 2016, **8**, 5226–5234.
- 4 R. Liu, Z. Zheng, J. Spurgeon and X. G. Yang, *Energy Environ. Sci.*, 2014, **7**, 2504–2517.
- 5 M. N. Ha, F. Zhu, Z. F. Liu, L. C. Wang, L. Y. Liu, G. Z. Lu and Z. Zhao, *RSC Adv.*, 2016, **6**, 21111–21118.
- 6 P. A. Bharad, K. Sivarajani and C. S. Gopinath, *Nanoscale*, 2015, **7**, 11206–11215.
- 7 C. Marchal, M. Behr, F. Vigneron, V. Caps and V. Keller, *New J. Chem.*, 2016, **40**, 4428–4435.
- 8 A. Iwase, S. Yoshino, T. Takayama, Y. H. Ng, R. Amal and A. Kudo, *J. Am. Chem. Soc.*, 2016, **138**, 10260–10264.
- 9 A. Fujishima and K. Honda, *Nature*, 1972, **238**, 37–38.
- 10 W. Zhou, W. Li, J. Q. Wang, Y. Qu, Y. Yang, Y. Xie, K. F. Zhang, L. Wang, H. G. Fu and D. Y. Zhao, *J. Am. Chem. Soc.*, 2014, **136**, 9280–9283.
- 11 S. Pany and K. M. Parida, *Phys. Chem. Chem. Phys.*, 2015, **17**, 8070–8077.
- 12 J. Fang, L. Xu, Z. Y. Zhang, Y. P. Yuan, S. W. Cao, Z. Wang, L. S. Yin, Y. S. Liao and C. Xue, *ACS Appl. Mater. Interfaces*, 2013, **5**, 8088–8092.
- 13 X. F. Zhang, B. Y. Zhang, Z. X. Zuo, M. K. Wang and Y. Shen, *J. Mater. Chem. A*, 2015, **3**, 10020–10025.
- 14 X.-Y. Liu, W.-D. Wei, S.-C. Cui and J.-G. Liu, *Catal. Lett.*, 2016, **146**, 1655–1662.
- 15 W. Q. Fang, Z. Y. Huo, P. R. Liu, X. L. Wang, M. Zhang, Y. Jia, H. M. Zhang, H. J. Zhao, H. G. Yang and X. D. Yao, *Chem. – Eur. J.*, 2014, **20**, 11439–11444.
- 16 W. Wang, Y. Liu, J. F. Qu, Y. B. Chen and Z. P. Shao, *RSC Adv.*, 2016, **6**, 40923–40931.
- 17 T. Wang, X. Q. Yan, S. S. Zhao, B. Lin, C. Xue, G. D. Yang, S. J. Ding, B. L. Yang, C. S. Ma, G. Yang and G. R. Yang, *J. Mater. Chem. A*, 2014, **2**, 15611–15619.
- 18 N. Liu, C. Schneider, D. Freitag, U. Venkatesan, V. R. R. Marthala, M. Hartmann, B. Winter, E. Spiecker, A. Osvet, E. M. Zolnhofer, K. Meyer, T. Nakajima, X. M. Zhou and P. Schmuki, *Angew. Chem.*, 2014, **126**, 14425–14429.
- 19 N. Liu, V. Häublein, X. M. Zhou, U. Venkatesan, M. Hartmann, M. Mačković, T. Nakajima, E. Spiecker, A. Osvet, L. Frey and P. Schmuki, *Nano Lett.*, 2015, **15**, 6815–6820.
- 20 R. Reichert, Z. Jusys and R. J. Behm, *J. Phys. Chem. C*, 2015, **119**, 24750–24759.
- 21 A. A. Melvin, K. Illath, T. Das, T. Raja, S. Bhattacharyya and C. S. Gopinath, *Nanoscale*, 2015, **7**, 13477–13488.
- 22 R. Kobayashi, S. Tanigawa, T. Takashima, B. Ohtani and H. Irie, *J. Phys. Chem. C*, 2014, **118**, 22450–22456.
- 23 F. L. Wang, Y. J. Jiang, D. J. Lawes, G. E. Ball, C. F. Zhou, Z. W. Liu and R. Amal, *ACS Catal.*, 2015, **5**, 3924–3931.
- 24 T. Ikeda, A. Xiong, T. Yoshinaga, K. Maeda, K. Domen and T. Teranishi, *J. Phys. Chem. C*, 2013, **117**, 2467–2473.
- 25 B. Banerjee, V. Amoli, A. Maurya, A. K. Sinha and A. Bhaumik, *Nanoscale*, 2015, **7**, 10504–10512.
- 26 P. Chowdhury, G. Malekshoar, M. B. Ray, J. Zhu and A. K. Ray, *Ind. Eng. Chem. Res.*, 2013, **52**, 5023–5029.
- 27 C. L. Muhich, Y. Zhou, A. M. Holder, A. W. Weimer and C. B. Musgrave, *J. Phys. Chem. C*, 2012, **116**, 10138–10149.
- 28 J. G. Yu, L. F. Qi and M. Jaroniec, *J. Phys. Chem. C*, 2010, **114**, 13118–13125.
- 29 G. J. Ai, R. Mo, H. X. Li and J. X. Zhong, *Nanoscale*, 2015, **7**, 6722–6728.
- 30 A. Meng, J. Zhang, D. Xu, B. Cheng and J. Yu, *Appl. Catal., B*, 2016, **198**, 286–294.
- 31 S. Bala, I. Mondal, A. Goswami, U. Pal and R. Mondal, *J. Mater. Chem. A*, 2015, **3**, 20288–20296.
- 32 T. Wang, X. G. Meng, G. G. Liu, K. Chang, P. Li, Q. Kang, L. Q. Liu, M. Li, S. X. Ouyang and J. H. Ye, *J. Mater. Chem. A*, 2015, **3**, 9491–9501.



- 33 S. M. Y. M. Mukthar Ali and K. Y. Sandhya, *RSC Adv.*, 2016, **6**, 60522–60529.
- 34 A. Y. Yermakov, G. S. Zakharova, M. A. Uimin, M. V. Kuznetsov, L. S. Molochnikov, S. F. Konev, A. S. Konev, A. S. Minin, V. V. Mesilov, V. R. Galakhov, A. S. Volegov, A. V. Korolyov, A. F. Gubkin, A. M. Murzakayev, A. D. Syvazhin and K. V. Melanin, *J. Phys. Chem. C*, 2016, **120**, 28857–28866.
- 35 R. Tang, Z. R. Xie, S. J. Zhou, Y. N. Zhang, Z. M. Yuan, L. Y. Zhang and L. W. Yin, *ACS Appl. Mater. Interfaces*, 2016, **8**, 22201–22212.
- 36 Y. J. Li, H. R. Yang, J. Tian, X. L. Hu and H. Z. Cui, *RSC Adv.*, 2017, **7**, 11503–11509.
- 37 A. Zielinska-Jurek, I. Wysocka, M. Janczarek, W. Stampor and J. Hupka, *Sep. Sci. Technol.*, 2015, **156**, 369–378.
- 38 C. Zhao, X. Shu, D. Zhu, S. Wei, Y. Wang, M. Tu and W. Gao, *Superlattices Microstruct.*, 2015, **88**, 32–42.
- 39 R. Jaiswal, N. Patel, A. Dashora, R. Fernandes, M. Yadav, R. Edla, R. S. Varma, D. C. Kothari, B. L. Ahuja and A. Miotello, *Appl. Catal., B*, 2016, **183**, 242–253.
- 40 C. Perego, Y. H. Wang, O. Durupthy, S. Cassaignon, R. Revel and J. P. Jolivet, *ACS Appl. Mater. Interfaces*, 2012, **4**, 752–760.
- 41 L. Zhang, X. H. Huang, J. S. Hu, J. Song and I. Kim, *Langmuir*, 2017, **33**, 1867–1871.
- 42 G. Dai, S. Liua, Y. Liang and T. Luo, *Appl. Surf. Sci.*, 2013, **264**, 157–161.
- 43 T. Wang, X. Meng, G. Liu, K. Chang, P. Li, Q. Kang, L. Liu, M. Li, S. Ouyang and J. Ye, *J. Mater. Chem. A*, 2015, **3**, 9491–9501.
- 44 S. Huang, Y. Yu, Y. Yan, J. Yuan, S. Yin and Y. Cao, *RSC Adv.*, 2016, **6**, 29950–29957.
- 45 S. G. Babu, R. Vinoth, D. P. Kumar, M. V. Shankar, H.-L. Chou, K. Vinodgopal and B. Neppolian, *Nanoscale*, 2015, **7**, 7849–7857.
- 46 J. J. Wu, S. L. Lu, D. H. Ge, L. Z. Zhang, W. Chen and H. W. Gu, *RSC Adv.*, 2016, **6**, 67502–67508.
- 47 P.-P. Sun, L. Liu, S.-C. Cui and J.-G. Liu, *Catal. Lett.*, 2014, **144**, 2107–2113.
- 48 Y. Chang, C. H. Yuan, Y. T. Li, C. Liu, T. Wu, B. Zeng, Y. T. Xu and L. Z. Dai, *J. Mater. Chem. A*, 2017, **5**, 1672–1678.
- 49 B. Huang, W. J. Yang, Y. W. Wen, B. Shan and R. Chen, *ACS Appl. Mater. Interfaces*, 2015, **7**, 422–431.
- 50 D. B. Hamal and K. J. Klabunde, *J. Phys. Chem. C*, 2011, **115**, 17359–17367.

